Extreme Mechanics Letters 55 (2022) 101827

Contents lists available at ScienceDirect

Extreme Mechanics Letters

journal homepage: www.elsevier.com/locate/eml

A physics-guided machine learning for multifunctional wave control in active metabeams

Jiaji Chen [a], Yangyang Chen [b], Xianchen Xu [a], Weijian Zhou [c,*], Guoliang Huang [a,*]

[a] Department of Mechanical and Aerospace Engineering, University of Missouri, Columbia, MO 65211, USA
[b] Department of Mechanical and Aerospace Engineering, The Hong Kong University of Science and Technology, Clear Water Bay, Hong Kong, China
[c] School of Science, Harbin Institute of Technology, Shenzhen, 518055, China

ARTICLE INFO

Article history:
Received 15 April 2022
Received in revised form 4 June 2022
Accepted 27 June 2022
Available online 30 June 2022

Keywords:
Active metabeams
Machine learning
Multifunctional wave control
Surrogate optimization

ABSTRACT

With the growing interest in the field of artificial materials, more advanced and sophisticated wave functionalities are required from phononic crystals and acoustic metamaterials. Due to expensive iterative fitness evaluations, inverse designing acoustic metamaterials with desired physical responses using conventional optimization approaches remains challenging especially in high-dimensional design space. To address this issue, we suggest a physics-guided machine-learning-based inverse design approach for realizing multifunctional wave control in active metabeams connecting with negative capacitances (NCs). The transfer matrix method which relates the wave field and its derivative to carry the fundamental wave propagation information will be embedded in the ML network to construct the complex mapping between the input and output responses of the unit cell. After this network is well trained, global wave propagation behavior in the active metabeam can be accurately described by the concatenation of networks of each unit cells into a global stiffness matrix. After the performance of the network is validated by conducting numerical simulation, we further apply the proposed network as a surrogate model for genetic algorithm on the inverse design of the metabeam for quick realization multifunctional wave control abilities without changing microstructures. Our proposed approach can not only be easily extended to design other types of active/passive metamaterials, but also provides some insights into optimization aided engineering in high-dimensional (2D and 3D) design space of active metamaterials.

1. Introduction

Mechanical metamaterials, which are artificially engineered materials, have shown promising potential for manipulating elastic waves at the subwavelength scale. Innovative methods for elastic wave focusing [1], cloaking [2], super-resolution imaging [3], negative refraction [4] and wave steering [5] have been explored. Nonetheless, there exist challenges that the capabilities of the passive metamaterials are not sufficient or extremely difficult to achieve various wave and vibration control applications because most engineering problems are broadband and very dynamic in nature. Moreover, actively controlling the position and width of the band-gap frequency region in real-time is very difficult in practice, if not impossible, for passive metamaterials. One of the most pronounced challenges in mechanical metamaterial development is the ability to tune their performance in an adaptive manner without requiring physical microstructural modifications. To tackle this challenge, the active metamaterials were developed by integrating smart materials into the microstructures of the passive metamaterials [6–8]. Among those works, piezoelectric patching techniques have demonstrated their outstanding potentials for achieving tunable properties and wave functionalities [9,10]. Due to their quick response, shunted or programmable electric circuits can tune the mechanical deformation of the metamaterial in real time. Many active metamaterials with piezoelectric patches have been proposed for broadband wave control, vibration mitigation, topological insulators and even odd elasticity by electrically tuning the dynamic stiffness, mass density, impedance and stiffness tensor [11–14]. For example, the active metabeams with semi-active negative capacitances (NCs) possess tunable band gaps or wave-guiding over desired broadband frequency ranges [15,16]. However, as an inverse design problem, there is still a lack of efficient approach to find a feasible active metabeam with non-periodic NCs for fulfilling multifunctional and multifrequency wave control capabilities. These abilities are crucial in many engineering scenarios ranging from wave steering to frequency selection in elastic wave detection and imaging.

The inverse designs of the mechanical metamaterials are mainly based on the optimization methods. For an example, to

* Corresponding authors.
E-mail addresses: zwj0607@zju.edu.cn (W. Zhou), huangg@missouri.edu (G. Huang).

https://doi.org/10.1016/j.eml.2022.101827
2352-4316/

find the band gap in a certain frequency range or the phase shift at a specific frequency, an optimization method (such as the genetic algorithm) can automatically search for an optimal solution in the design space [17–21]. Solving an optimization problem is convenient and straight forward. However, optimization algorithms are generally computationally intensive due to iterative fitness evaluations. Inverse design problems for multifunctional realization of the active metamaterial are extremely difficult or time-consuming if not impossible. In light of the aforementioned challenges, and driven by the progress in data science, promising alternatives have been surfaced in the form of machine learning (ML) techniques. The incorporation of ML into the inverse metamaterial design could significantly reduce computation efforts due to the training and reward mechanism. Recently, ML techniques have demonstrated their remarkable ability in unveiling the implicit relationship between the microstructures and the targeted wave responses of metamaterials [22–26]. Multilayer perceptron (MLP), also known as artificial neural network (ANN), have been widely used in ML techniques for inverse designs of the metamaterial for specific wave mitigation application [27–29]. The MLP network is powerful in building the nonlinear mapping relation from a complex input dataset to a complex output dataset [30]. Despite their towering empirical promise and some preliminary success, most ML approaches currently are unable to extract interpretable physical information and knowledge from this data deluge. Moreover, purely data-driven models may fit observations very well, but predictions may be physically inconsistent or implausible, owing to extrapolation or observational biases that may lead to poor generalization performance. Therefore, there is a strong need for integrating fundamental physical laws and domain knowledge by 'teaching' ML models about governing or underlying physical rules, which can, in turn, provide 'physics information' — that is, strong theoretical constraints and inductive biases on top of the observational ones. To this end, physics-guided learning as the process by which prior knowledge stemming from the physical modeling can be leveraged to improve the performance of a ML algorithm. Currently, there is only limited work on physics based ML model. For instance, Samaniego et al. [31] and Anitescu et al. [32] proposed to use ANN to solve classical partial differential equations that govern certain physical mechanisms. However, these works primarily target on solving physics field distribution, rather than the inverse design of materials.

In this study, a physics-guided ML technique is proposed to seek an inverse solution of the active metabeam for various wave control abilities by integrating non-periodic piezoelectric patches with different NCs. We aim at designing an inhomogeneous 1D active metabeam consisting of dissimilar unit cells capable of achieving user-defined dynamic performance. The transfer matrix method which relates the wave field and its derivative to carry the fundamental wave propagation information will be embedded in the ML network to construct the complex mapping between the input and output responses of the unit cell. After this network is well trained based on a small dataset, global wave propagation behavior in the active metabeam can be accurately described by the concatenation of networks of each unit cells into a global stiffness matrix of the entire beam. Therefore, the network in our approach can completely replace the original physical model, where its input and output are left-end and right-end responses of the metabeam. The performance of the network is validated by conducting numerical simulation on predicting the global wave field of the active metabeam. We further apply the proposed network as a surrogate model for genetic algorithm (GA) on the inverse design of the metabeam for quick realization of multifunctional wave control abilities, which is difficult and time consuming for standard optimization method. It is worth mentioning that the proposed ML-based approach requires only a one-time network training on unitcell to model the entire metabeam structure. The design parameters of each individual element are then determined through the GA-based inverse design. Such design method of the active metamaterial based on the machine learning techniques can easily extend to the high dimension problem, which will find potential applications in fast design of active acoustic devices and complex multiple-functional metamaterial systems.

2. Construction of physics-guided ML model of a 1D active metabeam

2.1. Physics modeling of active metabeam

As illustrated in Fig. 1(a), the active metabeam is constructed by bonding an array of piezoelectric (PZT-5A) patches to a host beam. The patches are individually shunted with an array of different NC circuits to ensure a variation in the refractive index, whose impedance is $Z = 1/(iC_N\omega)$ with $i = \sqrt{-1}$. Fig. 1(b,c) show the nth unit cell of the active metamaterial beam and the schematic of its shunted NC circuit, respectively. The value C_N of each NC can be expressed as $C_N = -\frac{R_1}{R_2}C_0$, with C_0 being a referential capacity. Thus, by changing the variational resistance R_1, the negative capacitance C_N, or equivalently, the negative capacitance ratio (NCR) $\lambda = C_N/C_P^T$, can be continuously tuned, allowing ones to continuously modify the effective material properties of the metamaterial over a broad frequency range. Here, C_P^T is the capacitance of the piezoelectric plate under constant stresses.

For the direct problem, the multiphysics model is formulated to calculate the effective bending properties of the piezoelectric plate by considering electro-mechanical coupling and the transfer matrix method is employed to study wave propagation of the system. We start with a brief review of a linear metabeam governed by an equation of motion [33]. For a homogeneous thin beam, the motion equation governing the flexural wave propagation can be written by the Euler–Bernoulli beam theory as:

$$EI\frac{\partial^4}{\partial x^4}w - \rho S\omega^2 w = 0 \tag{1}$$

where EI is the flexural stiffness, ρ is the mass density, S is the cross-section area, and w is the deflection of the beam. By using the transfer matrix method, we can obtain the transfer relation as:

$$\xi_{\mathbf{R}} = \mathbf{Q}\xi_{\mathbf{L}} \tag{2}$$

where ξ is the state vector defined as $\xi = (w\ \theta\ M\ F)^T$, θ is the rotation angle, M is the bending momentum, F is the shearing force, the subscript L and R denote the parameters at left and right end, respectively, and $\mathbf{Q}$ is the transfer matrix that builds the relation between the left state vector and the right state vector. The transfer matrix $\mathbf{Q}$ contains all the key mechanical characteristics that determine the wave transmission and reflection at the beam unit. For a homogeneous thin beam considered above, the transfer matrix can be explicitly obtained. However, it is difficult to obtain its explicit expression for the active metabeam with complex microstructures and multiphysics coupling.

The transfer matrix $\mathbf{Q}$ of the active metabeam can be numerically obtained from effective homogenization approach which is only suitable for low-frequency wave propagation [33]. To overcome the limitation, we numerically calculate 16 components Q_{ij} of the transfer matrix from the commercial software COMSOL Multiphysics. The FEM model consider both the piezoelectric device module and the electric circuit module in frequency domain. To numerically obtain the values of 16 components Q_{ij} for a given

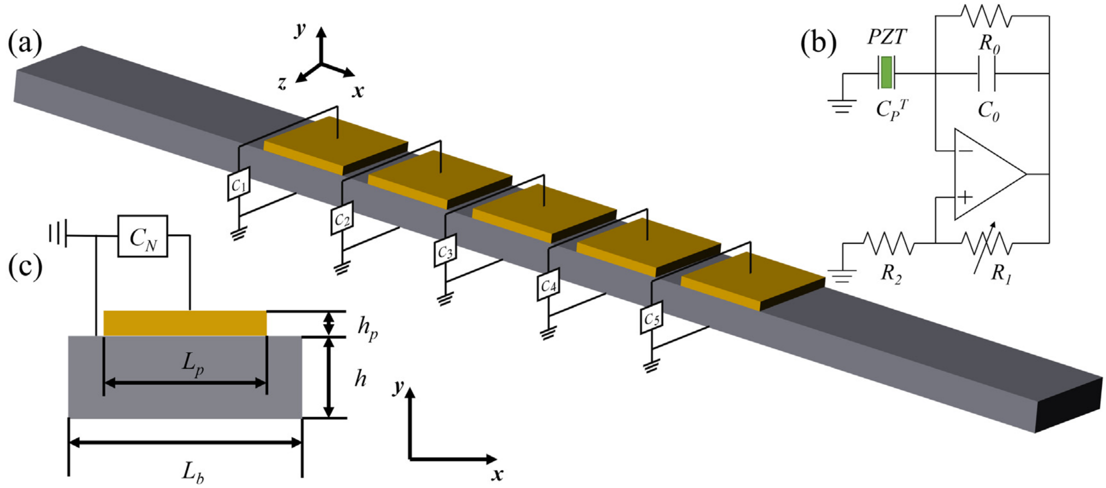

Fig. 1. Schematic of the active metabeam. (a) A host beam is bonded with an array of piezoelectric (PZT-5A) patches, which are shunted by NC circuits to realize an adaptive wave control. (b) Schematic of the NC shunting circuit, which consists of an operational amplifier, two resistors, a capacitor, and a potentiometer. By adjusting the resistance of the potentiometer, the equivalent NC of the circuit can be altered. (c) Schematic of the unit cell of the active metabeam. For simplicity, the propagation of flexural waves is assumed to be confined along the x direction.

working frequency ω and a negative capacitance C_N, we need 16 equations. The FEM simulations with 4 groups of independent boundary state vectors are then conducted as (1) $w_L = 1$, $\theta_L = 0$, $w_R = 0$ and $\theta_R = 0$; (2) $w_L = 0$, $\theta_L = 1$, $w_R = 0$ and $\theta_R = 0$; (3) $w_L = 0$, $\theta_L = 0$, $w_R = 1$ and $\theta_R = 0$; and (4) $w_L = 0$, $\theta_L = 0$, $w_R = 0$ and $\theta_R = 1$. Based on the calculated components M_L, F_L, M_R and F_R, the transfer matrix in the metabeam unit can be numerically determined. As a result, the global transfer matrix for the metabeam with n unit cells can be then expressed as:

$$\mathbf{Q_G} = \mathbf{Q}(n)\mathbf{Q}(n-1)\cdots\mathbf{Q}(2)\mathbf{Q}(1) \tag{3}$$

The global transfer matrix relates the state vector ξ_{GR} at the right end of the metabeam with the state vector ξ_{GL} at the left end of the metabeam via $\xi_{GR} = \mathbf{Q}_G\xi_{GL}$, from which we can calculate the transmission of the flexural wave propagating through this system. (See details in Appendix)

2.2. Physics-guided ML network

In this section, we construct a group of ML networks to learn and predict the transfer matrices of these active metabeam unit cells. In the study, the host beam is made with aluminum (mass density $\rho = 2700.0$ kg m^{-3}, Young's modulus $E = 69.0$ Gpa, Poisson's ratio $\nu = 0.33$). The piezoelectric material is PZE-5A (mass density $\rho = 7750.0$ kg m^{-3}, elastic compliance $s^E_{11} = 16.4 \times 10^{-12}$ m^2 N^{-1}, dielectric constant $\epsilon^T_{33} = 1700\epsilon_0$, piezoelectric constant $d_{31} = 171 \times 10^{-12}$ pC N^{-1}). The dimension of the unit cell we use here has $L_b = 10$ mm, $L_p = 9$ mm, $h = 1.6$ mm, $h_p = 0.9$ mm, as labeled in Fig. 1. As the first step, we produce a dataset by conducting the numerical simulation. According to Hagood and von Flotow [34], the normalized effective modulus of shunted piezoelectric patches $E_{eff} = E^s/E^d$ can be analytically obtained in function of the NCR [11]. When λ approaches to $-(1-k^2_{31})$ from small negative values, the effective modulus approaches positive infinity. However, when λ approaches to $-(1-k^2_{31})$ from large negative values, the effective modulus is changed from a positive value to a negative value, and eventually approaches negative infinity, where k_{31} denotes the electromechanical coupling coefficient. Thus, to better learn the mapping relation of effective modulus of piezoelectric patches, we intentionally sample more frequently when NCR is close to the instability limit. The distribution of the sample data density as functions of the frequency and negative capacitance is shown in Fig. 2(b)

Fig. 3 shows the schematic of our multiple layer perception (MLP) neural networks and their assembly to form the global transfer matrix prediction network for a user-defined target dynamic behavior. As illustrated in Fig. 3(a), a MLP network is trained to learn the physics within a unit cell. Thousands of working frequencies ω and NCRs λ are imported into FEM simulations in sequence, and therefore we can numerically calculate the components of the corresponding transfer matrix $\mathbf{Q}$ that determines dynamic behavior of the metabeam. Since effective Young's Modulus change rapidly as NC approach some certain critical value, elements of transfer matrix increase/decrease rapidly as well. The working frequencies and electrical impedances are used as input datasets, while the corresponding transfer matrices are used as output datasets. Then these input and output dataset are fed into the MLP model, allow it to learn the mapping of a metabeam unit from frequency and impedance to the corresponding transfer matrix. Similar to effective Young's Modulus, elements of transfer matrix experience discontinuity from negative infinity to infinity (or vice versa). If we train a single neural network to predict dynamical response of a broad range of NCRs, the neural network would potentially lead to a poorly trained model since most of ML algorithms assume inputs in continuous spaces. To circumvent the unnecessary penalty to NN accuracy, we trained 2 neural networks: one corresponding to softening circuit and the other to stiffening circuit. We generated 5000 data samples each for softening and stiffening circuits, which are split into 3 distinct groups: 80% samples for training, 10% for validation, and the rest 10% for testing. The training data are used to train the network by optimizing parameters within neural network, while the validation dataset serves for checking and avoiding the overfitting issue, and the testing dataset examines the prediction accuracy of the network. The network consists of four layers, i.e., one input layer, two hidden layers, and one output layer. The network training is achieved through standard back propagation algorithm [30]. After this MLP network being well trained, we assemble multiple neural networks to determine the global transfer matrix via Eq. (3) to predict the dynamic response along the entire active beam system, as sketched in Fig. 3(b). Assuming the metabeam consists of n units, given the input responses at the left end of the bar, the wave frequency, and the output responses at the right end of the metabeam, the design parameters (i.e., the negative capacitance of each unit) are obtained.

In particular, the network is generated and trained by the *fitnet* function in MATLAB, and the Levenberg–Marquardt (LM)

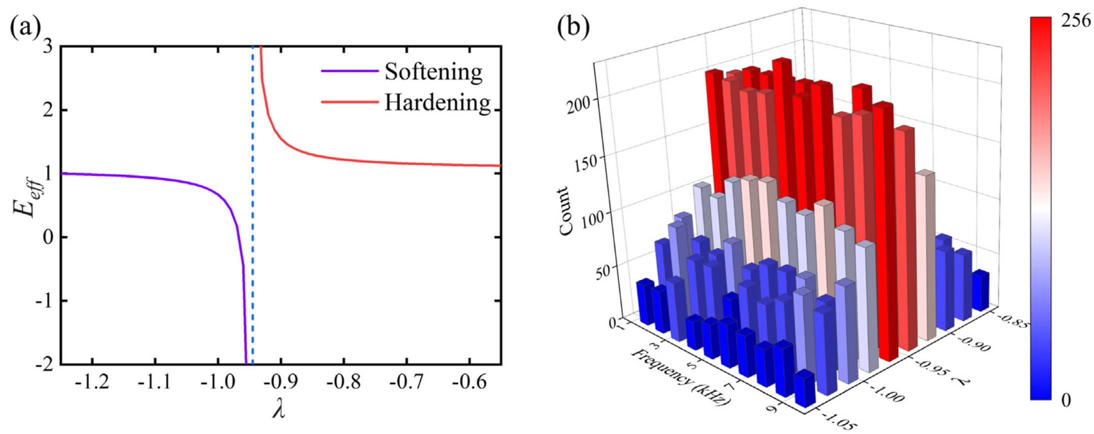

Fig. 2. (a) Normalized effective Young's modulus of piezoelectric patches with different negative capacitances. (a) The data distribution with different negative capacitances and frequencies.

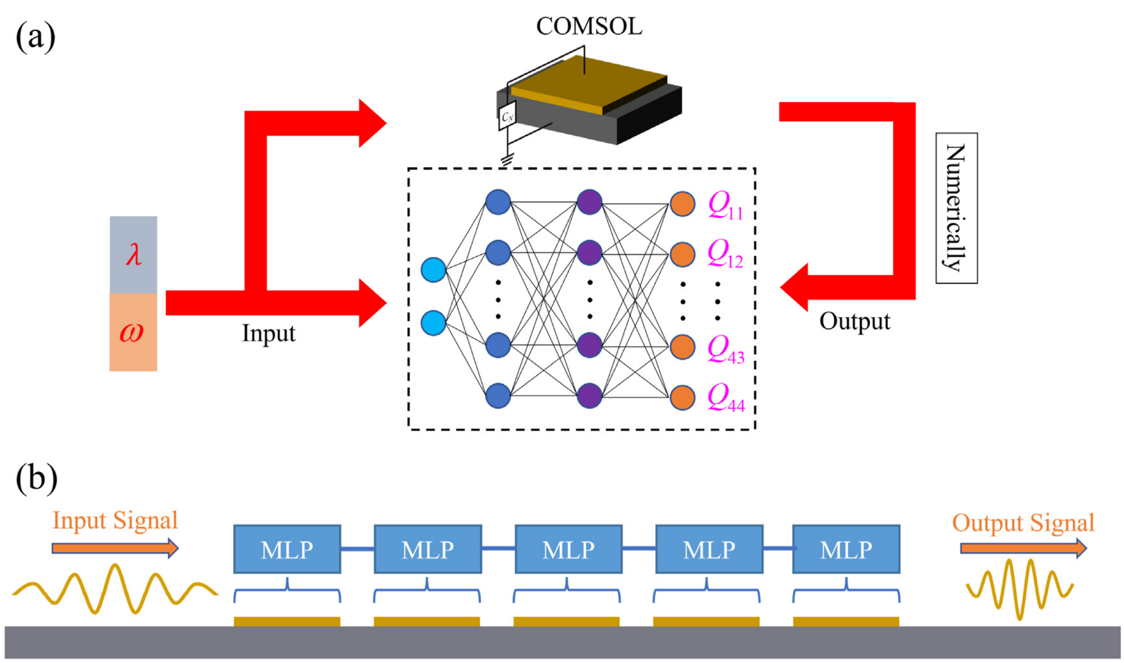

Fig. 3. The ML network for prediction of global transfer matrix components. (a) The sketch of the ML network for a metabeam unit: the electrical impedance and the frequency are imported into COMSOL simulation, from which the transfer matrix is calculated. (b) The ML networks to obtain the global transfer matrix based on Eq. (3).

optimizer is adapted to achieve accurate prediction of the transfer matrix. LM optimization, also known as the damped least-squares method, is a nonlinear optimization algorithm which is a combination of gradient descent and the Gauss–Newton. The update rule for LM optimization is expressed as:

$$\mathbf{w}_{i+1} = \mathbf{w}_i - (\mathbf{H} + \lambda \times diag(\mathbf{H}))^{-1}\mathbf{d} \quad (4)$$

where $\mathbf{w}_i$ is the weight within ith layer, $\mathbf{d}$ stands for derivative and $\mathbf{H}$ stands for Hessian. Levenberg–Marquardt optimizer has been proven to be more precise comparing with most of other common backpropagation algorithms, including stochastic gradient descent (SGD) and Adams [35].

The history of the obtained the mean square error (MSE) over the number of the samples is illustrated to training process of the network shown in Fig. 4(a). The MSE is defined as

$$MSE = \frac{1}{N}\sum_n (\vec{f}^n_{predict} - \vec{f}^n_{true})^2 \quad (5)$$

where $\vec{f}^n_{predict}$ is the predicted 16 components of the transfer matrix from the ML network, $\vec{f}^n_{true}$ is the values from the FEM, and N is the total number of the samples in an epoch. The structure of our MLP network is given as [2 30 30 16] neurons in each layer, while the 2 neurons in the input layer represent NCR and wave frequency, and the 16 neurons in the output layer represent for 16 transfer matrix elements. It is noticed that the network is well trained since the MSEs of training and validation data are very small after 300 epochs' training. The testing errors of the network are presented in Fig. 4(b). We can see that most of relative error lie under 0.002%, which means that the neural network has reached extreme level of precision. The reason we pursue this

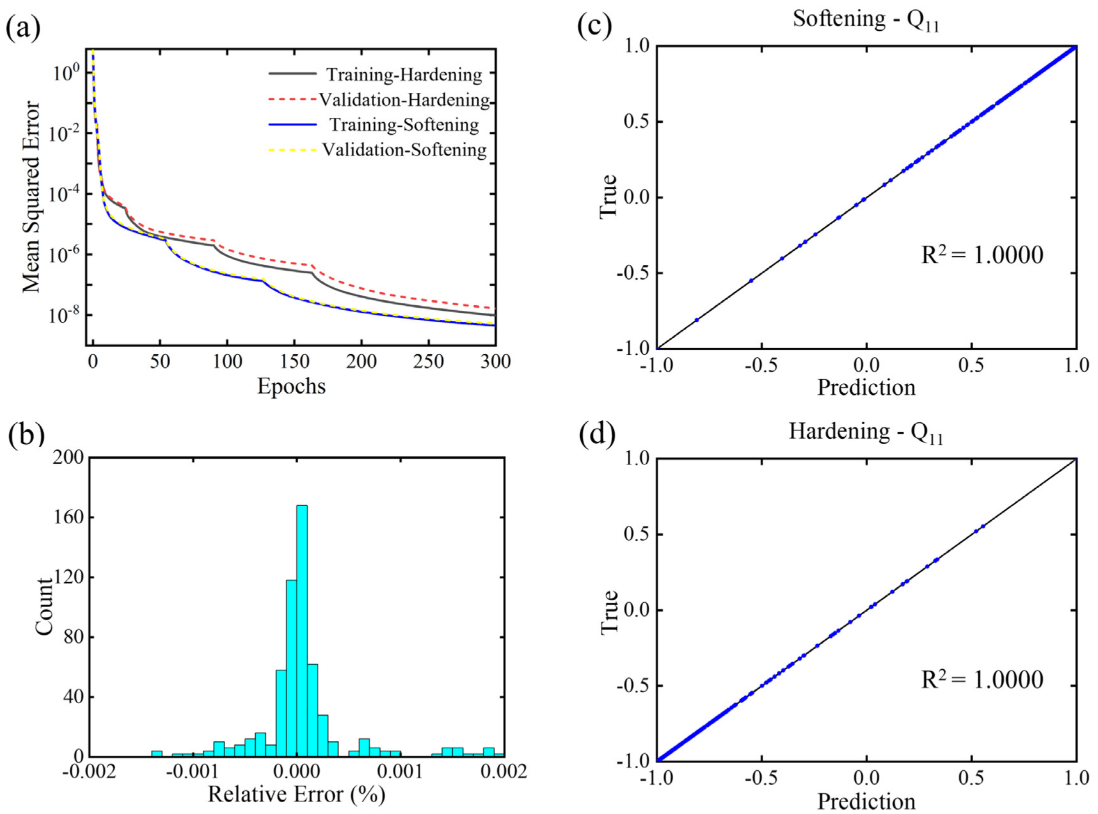

Fig. 4. (a) The history of the obtained MSE values over the number of the samples to illustrate training process of the ML network. (b) Histogram of the relative error for the testing data samples. The relative error here is defined as $x = \sum_n ((\vec{f}^n_{predict} - \vec{f}^n_{true})/\vec{f}^n_{true})$. The testing data samples here include testing samples for both softening circuit network and stiffening circuit network. (c) Comparison of the ML predicted Q_{11} component of the transfer matrix for softening circuits with the FEM results. (d) Comparison of the ML predicted Q_{11} component of the transfer matrix for hardening circuits with the FEM results. The corresponding The R^2 deviations are indicated.

level of precision is that we need to perform matrix multiplication while concatenating matrices to obtain global transfer matrix. During multiplication, any small error would be amplified and propagate through the entire active metabeam system, and thus provide inaccurate prediction of metabeam dynamics. The error would continue to accumulate and amplify as we perform further calculations (as we will do in the inverse design section). We compared our current model with standard regression method, for instance, linear regression and ANN trained with Adam optimizer, and result shows that the proposed MLP model is indeed superior than other methods (see more details in Appendix). This further emphasize our choice of using LM optimizer, which allow us to raise prediction accuracy to an extreme level for a neural network. Fig. 4(c) and (d) show the comparison between ML predicted Q_{11} component of the transfer matrix and the FEM calculated one. R^2 deviations in both stiffening and softening circuits are 1.0000, which further testify the extreme precision of our trained network.

To validate the accuracy of the ML network, the mechanical responses of a metabeam system with NCs at 10 kHz will be studied by calculating ML-based global transfer matrix. The two examples of the active metabeam with ten distributed NCs in both softening and hardening circuits are considered as:

$$\textit{Case } 1 : [\lambda_N] = -(1.500,\ 1.400,\ 1.300,\ 1.200,\ 1.100,\ 1.000,\ 0.990,\ 0.980,\ 0.970,\ 0.960)$$

$$\textit{Case } 2 : [\lambda_N] = -(0.940,\ 0.930,\ 0.920,\ 0.910,\ 0.900,\ 0.890,\ 0.880,\ 0.870,\ 0.860,\ 0.850)$$

with boundary condition $M_0 = 0$, $F_0 = 1$, $M_{10} = 0$ and $F_{10} = 0$. The state vectors ξ in the metabeam system from both network predictions and the direct FEM simulations are shown in Fig. 5. The distribution of nodal number across the beam is defined in Fig. 5(a). The distributions of nodal deflection, nodal rotational angle, nodal bending moment and nodal shearing force are shown in Fig. 5(b) for case 1 and in Fig. 5(c) for case 2, respectively. The red dashed curves are calculated from the FEM simulations, while the gray dots are from the ML networks. The predictions from the ML networks are in excellent agreement with those from FEM simulations, meaning that the network is well trained and ready to predict the dynamic behaviors of the active metabeam if the frequency and negative capacitance array are given.

3. Fast inverse design by ML-based surrogate optimization

The proposed ML framework is then employed on the inverse design of the 1D active metabeam for a user-defined output wave responses within the desired wave frequency range to realize the multifunctional wave control abilities. The most remarkable characteristic of this approach lies in its ability to build predictive models of complex dynamical systems from the use of basic (previously trained) networks. Fig. 6 illustrates the well-trained ML model as a surrogate model to replace the FEM simulations in the traditional optimizer, making the inverse design extremely fast. The objective of the training is to achieve desired wave transmissions at different frequencies by identify the NCs while

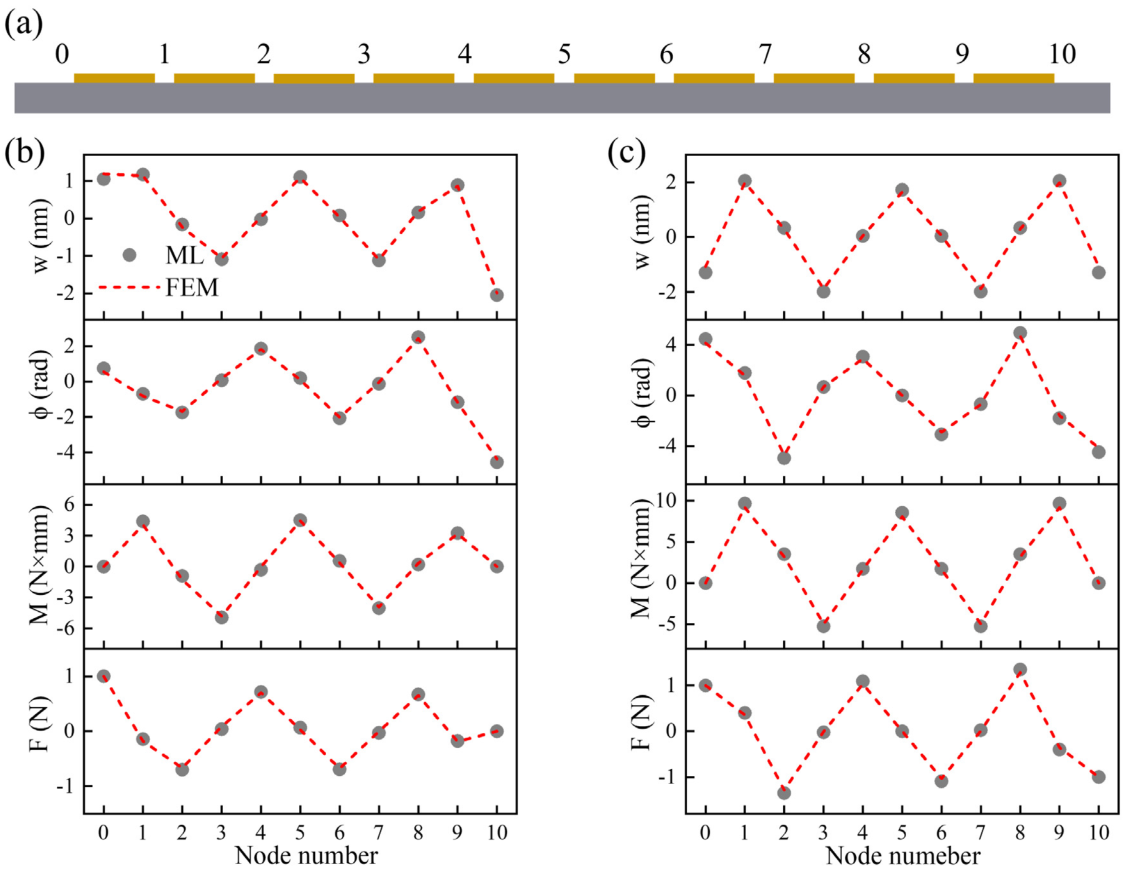

Fig. 5. Comparison of state vectors ξ prediction of the active metabeam from between the ML network and the FEM simulations. (a) The nodal numbers defined in the metabeam system. (b) The ξ distribution of nodal deflection w, rotation angle θ, bending momentum M and shearing force F in case 1 and, (c) the ξ distribution in case 2.

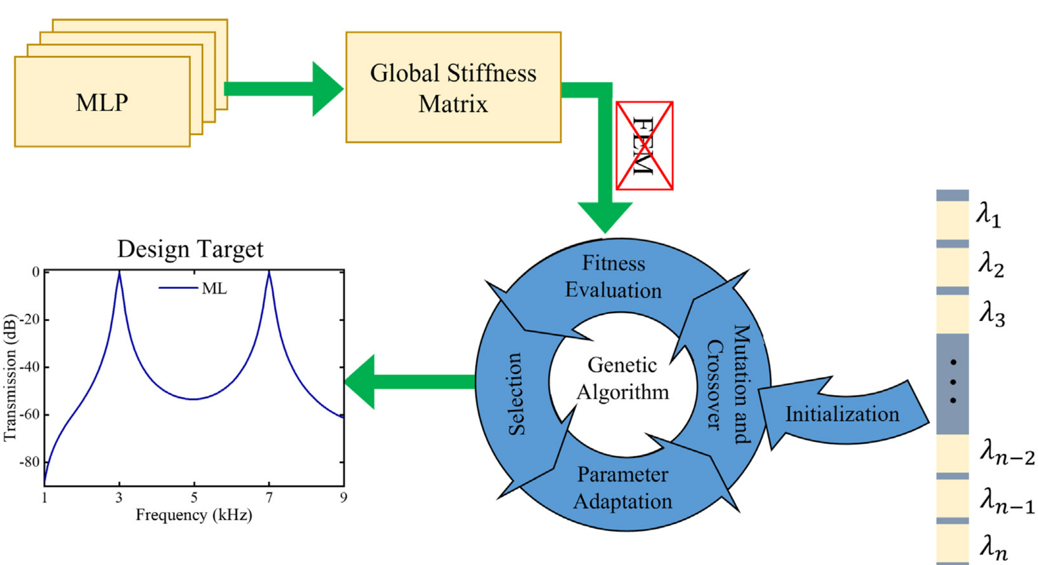

Fig. 6. Comparison of state vectors ξ prediction of the active metabeam from between the ML network and the FEM simulations. (a) The nodal numbers defined in the metabeam system. (b) The ξ distribution of nodal deflection w, rotation angle θ, bending momentum M and shearing force F in case 1 and, (c) the ξ distribution in case 2.

keeping the dimension and the length of the active metabeam unchanged.

Specifically, we apply genetic algorithm (GA) on the trained network to inverse design a multiple-functional waveguide of the metabeam composing of 10 independent active NC units. The wave transmission for the frequency range (from 1 kHz to 10 kHz) can be obtained by employing the global transfer matrix from ML networks. As an inverse design example, the 10 NCs

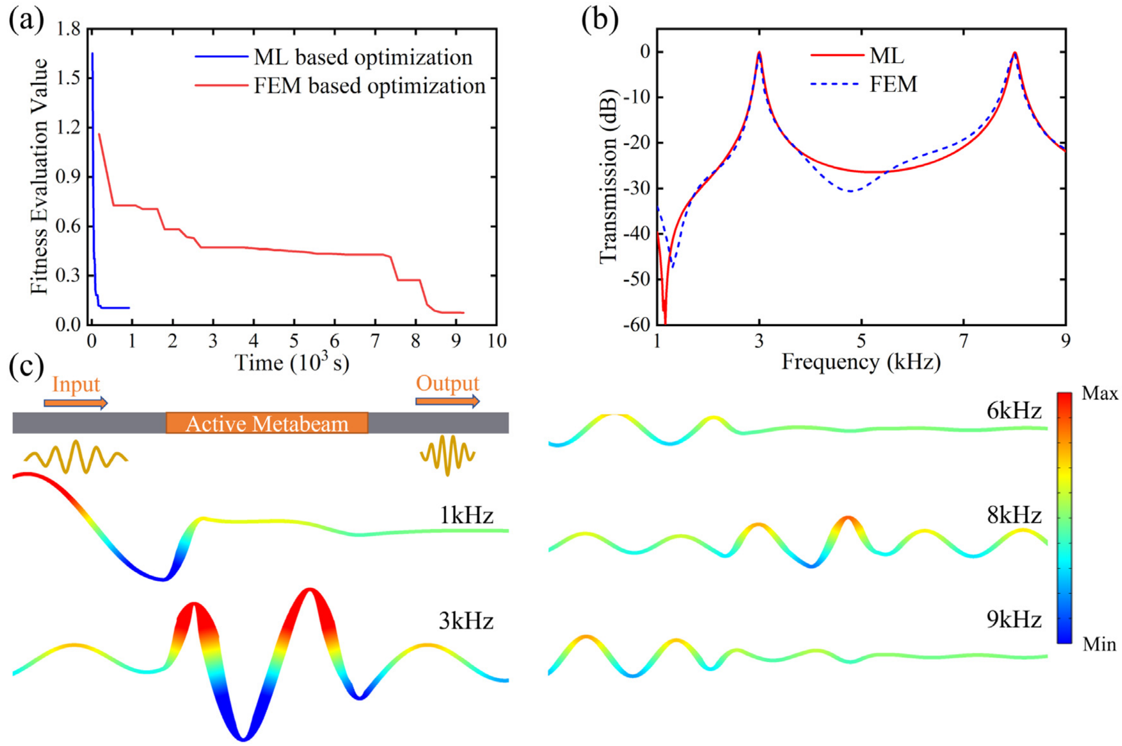

Fig. 7. (a) Time history of the fitness evaluation values from the ML-based surrogate optimization and FEM-based classical optimization. (b) Transmission profile in function of the frequency from ML network prediction and FEM simulations according to the objective function q_1. (c) Harmonic wave transmission in the active metabeam at different frequencies.

in the active metabeam are treated as design parameters for the targeted wave transmission, which is expected to be maximized at frequencies 3 kHz and 8 kHz, while minimized at frequencies 1, 6 and 9 kHz, respectively. To the end, the objective function of the optimization problem can be described as

$$\min: \quad q_1(\lambda_1, \lambda_2, \ldots, \lambda_{10}) = T(1) - T(3) + T(6) - T(8) + T(9) \quad (6)$$

where the wave transmission here is defined as $T = 20\, log(U_{out}/U_{in})$ with U_{out} and U_{in} being the output and incident displacement amplitudes in the host beam. At this point, 10 identical NNs are concatenated to model the dynamic behavior of the metabeam, and the NCs are determined by solving Eq. (3). It should be mentioned that the metabeam with different NCs distribution could be generated from the inverse surrogate optimization. However, the physics mechanism will be the same unregard of NC's distribution across the metabeam.

Starting with an initial guess for the negative capacitance, the ML algorithm iteratively searches for the optimal NCs based on the objective function estimated from the ML model instead of the FEM simulation. The process is implemented iteratively and the agent will continue exploring the design space until the termination condition (fitness evaluation q is converged to the minimized value) is reached. The design process is completed once the dynamic behavior of the synthesized metabeam satisfies a user-defined wave transmission tolerance. To demonstrate the advantages of the ML-based surrogate optimization, the comparison of the optimization processing time between the ML-based surrogate optimization and the classical FEM-based optimization is shown in Fig. 7(a). It can be concluded that the surrogate optimization based on the ML trained networks only need 100 s to reach an optimal design, however, the classical optimization takes at least 9000 s to find an optimal design. Therefore, the surrogate optimization can significantly speed up the inverse design to locate the active metabeam with different NCs for user-defined wave functions. As a result, the proposed ML-based approach is preferred whenever an online inverse design is necessary and the behavior of the metamaterial is well-understood. To evaluate the accuracy of the proposed ML-based optimization, the wave transmission behaviors of the metabeam in the desired frequency range from the ML network are presented in Fig. 7(b), in which the ten NCs are inversely determined as $-[1.0481, 0.9531, 0.9450, 1.0258, 0.9950, 0.8710, 0.9850, 0.9693, 0.9328, 0.9447]$. The transmission peaks at frequencies 3 and 8 kHz are evidenced and the transmission dips at frequencies 1, 6 and 9 kHz are observed, which indicates that the surrogate optimization does obtain an optimal design to meet the target. For comparison, the exact wave transmission of the metabeam with the predicted NCs are also calculated from FEM simulations, which are plotted as the red solid curve. Very good agreement on the wave control behavior is clearly seen. To quantitatively demonstrate wave propagation of the metabeam at interested wave frequencies, the harmonic wave analyses are conducted at discrete frequencies, which is shown in Fig. 7(c). The wave propagation is forbidden at 1, 6 and 9 kHz, and most of the wave energy have been transmitted through the active metabeam with 10 units. The wave attenuation can be attributed to the multiple scattering attenuation mechanism in the resulting heterogeneous beam caused by connecting to different NCs with softening and hardening circuits. However, for the frequencies at 3 and 8 kHz, the NCs could not produce any hindrance to flexural wave propagation with high transmission. To closely observe wave fields in 7(c) at frequencies 3 and 8 kHz, the wave transparency can be interpreted as the phononic cavity and Fabry–Perot resonance in this layered medium, respectively [36–38].

Different from the passive metabeams, the active metabeams can reconfigure their wave control functionalities by electrically changing NCs' circuits without the need of the change of microstructures. To accomplish this reconfigurable wave control

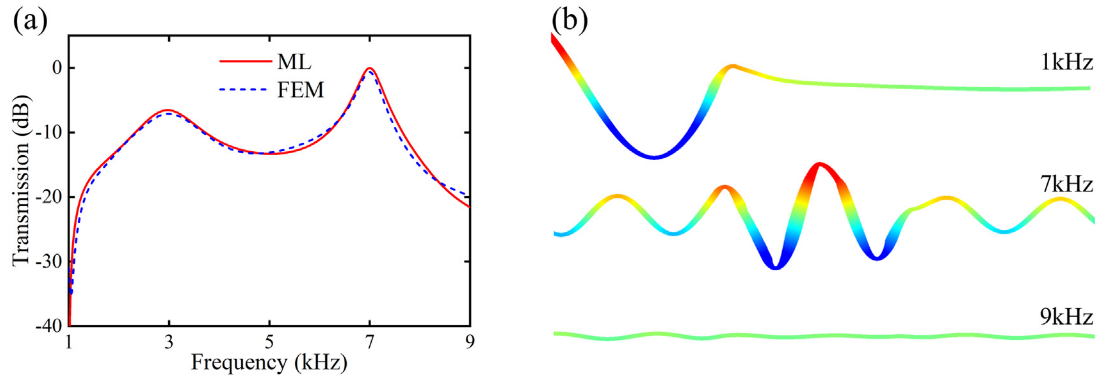

Fig. 8. (a) Transmission profile in function of the frequency from ML-based surrogate optimizations and FEM simulations according to the objective function q_2. (b) Harmonic wave transmission in the active metabeam at different frequencies.

abilities, a modified electrical system with different NC's distribution needs to be quickly determined. However, conventional algorithms are computationally intensive and becomes an obstacle toward practical applications. On the other hand, our proposed ML approach could meet this critical need and be used to identify this inverse solution in real time and fast fashion. For an instance, the new wave control function of the metabeam is to filter out the waves at frequencies 1 and 9 kHz, but allow the wave at 7 kHz to pass through the system with little decay. Based on the surrogate optimization, the optimization objective function is defined as:

$$\min: \quad q_2(\lambda_1, \lambda_2, \ldots, \lambda_{10}) = T(1) - T(7) + T(9) \tag{7}$$

where the 10 NCs are inversely determined as −[0.9760, 0.9441, 0.9013, 0.9930, 1.0449, 0.8692, 0.9075, 1.0229, 0.9284, 0.9970]. The wave transmission for the optimized metabeam calculated from ML model and FEM simulations are shown in Fig. 8(a). The wave control function of the metabeam is indeed realized by finding the wave transmission peak at 7 kHz and the wave transmission dips at 1 and 9 kHz and very good agreement is observed in comparison with the physical model. The harmonic wave simulation is also conducted to demonstrate this wave control function, as shown in Fig. 8(b).

It is worth mentioning that the differences between predictions and FEM in Figs. 7 and 8 are much larger than results shown in Fig. 6. The reason behind it is that we defined wave transmission as $T = 20log(U_{out}/U_{in})$. The difference mostly occurs at region below −20 dB, where the error is almost negligible if we define it as $T = U_{out}/U_{in}$. Furthermore, error accumulates as we assemble the global stiffness matrix, so that even a small error in predicting matrix element can be seen from the wave transmission in some cases.

To probe the dynamics wave phenomenon from NC technique, and to further examine the robustness of our proposed approach, we conduct time domain simulation, in which we excite flexural waves in the metabeam using piezoelectric actuators. We apply a tone burst signal centered at 9 kHz and attempt to design NC circuits that gives specific wave transmission. We independently retrieve the NC parameters for $T(9) = 1.0, 0.8, 0.6, 0.4, 0.2, 0.0$. Following the same scheme as in previous sections, we can obtain the NCR values from GA optimization as listed in Table 1. We then conduct the FE simulation with these NCs and check the physical response. The comparison between input signals and the detected pulses are shown in Fig. 9. As illustrated in Fig. 9, the transmitted wave signals are indeed our target wave responses from the ML.

Previous examples demonstrate our model's ability to manipulate wave transmission in a discrete manner. We may also extend it to a continuous domain by inversely designing the bandgap in a given frequency interval (f_{min}, f_{max}). The objective function of the optimization is defined as:

$$\begin{aligned} \min: \quad & q_3(\lambda_1, \lambda_2, \ldots, \lambda_{10}) = \int_a^b T(f)df \\ \text{s.t.} \quad & T(f) > T_{threshold} \quad \forall \quad f \in [f_{min}, a] \cup [b, f_{max}] \end{aligned} \tag{8}$$

where a and b are the lower bound and upper bound of the desired frequency region with minimized wave transmission, respectively. $T_{threshold}$ here is set to −2 dB. f_{min} and f_{max} are the lower bound and upper bound of the working frequency, in this case, 1 kHz and 10 kHz, respectively. In this study, we choose $a = 3$ kHz and $b = 7$ kHz. The optimization result shown in Fig. 10 indeed illustrates the accuracy of the proposed inverse design as the continuous transmission dip can be observed, in which the ten NCRs are inversely determined as −[0.9760, 0.9441, 0.9013, 0.9930, 1.0449, 0.8692, 0.9075, 1.0229, 0.9284, 0.9970].

Another interesting application of the inverse design is to achieve the rainbow trapping effect in the designed gradient index metabeam. Rainbow trapping refers to the wave phenomenon of separating different frequency wave components and spatially trapping them in different positions across the active metabeam [39–41]. By assigning the target cutoff frequencies in a gradient fashion, the objective function of the inverse design can be expressed as follows:

$$\min: \quad q_4(\lambda_1, \lambda_2, \ldots, \lambda_{10}) = |f_c - \hat{f}_c| \tag{9}$$

where f_c and $\hat{f}_c$ are 1×10 vectors of the predicted and target cutoff frequencies distribution from first unit cell to the last, respectively. In the study, the target cutoff frequencies linear distribution along the metabeam is assumed in Fig. 11(a). Note that the cutoff frequency of the first unit cell is not plotted because it is not within the working frequency of our physics-guided neural network. The predicted transfer matrix from the physics-guided neural network, together with the Floquet–Bloch theorem, is used to inversely determine the band structure associated with a given unit cell. To quantitatively validate the rainbow trapping effect, wave displacement distribution fields in the metabeam under harmonic loading are illustrated in Fig. 11(b) over different frequencies, in which the ten NCs are inversely determined as −[1.0512, 0.9512, 0.9505, 0.9499, 0.9494, 0.9489, 0.9486, 0.9482, 0.9480, 0.9479]. As shown in the figure, it is evident that the flexural wavelength gradually decreases in the metabeam at all frequencies., which renders a spatial compression of the flexural wave. It is worth mentioning that rainbow trapping effect has been validated in Ref. [33]. It can be concluded that the ML-based optimization is convenient, fast and accurate for realization of inverse design of reconfigurable and multi-functional wave devices.

Table 1
10 Negative capacitance ratio (NCR) for corresponding wave transmission.

Wave transmission	NCR (from left to right) 1	2	3	4	5	6	7	8	9	10
1.0	−1.0033	−1.0030	−0.9825	−0.9823	−0.9669	−0.9669	−0.9652	−0.9647	−0.9627	−0.9618
0.8	−1.0099	−1.0026	−0.9638	−0.9861	−0.9558	−0.9702	−0.9822	−0.9641	−1.0134	−1.0038
0.6	−0.9510	−1.0078	−0.9510	−0.9510	−1.0510	−0.9510	−0.9632	−0.9510	−0.9510	−1.0447
0.4	−0.9512	−0.9539	−1.0450	−0.9824	−0.9824	−0.9609	−0.9978	−1.0055	−0.9635	−1.0444
0.2	−0.9511	−1.0430	−0.9510	−0.9607	−0.9607	−0.9510	−1.0422	−0.9811	−0.9518	−1.0119
0.0	−1.0435	−1.0278	−0.9786	−0.9969	−0.9969	−1.0335	−1.0420	−0.9848	−0.9673	−1.0229

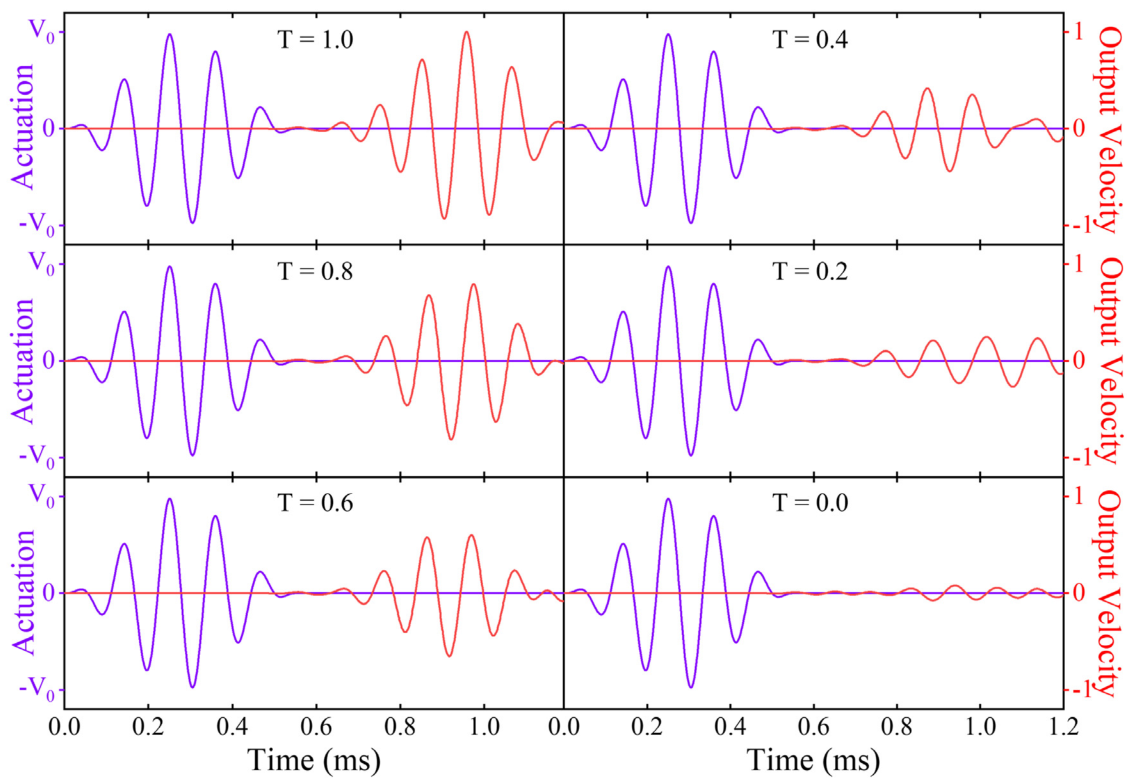

Fig. 9. Time domain simulation of flexural waves in the target active metabeams with different transmissions. A n = 5 cycles tone burst signal centered at f = 9 kHz is generated. The input voltage (violet) and output velocity (red) are normalized by their maximum values. (For interpretation of the references to color in this figure legend, the reader is referred to the web version of this article.)

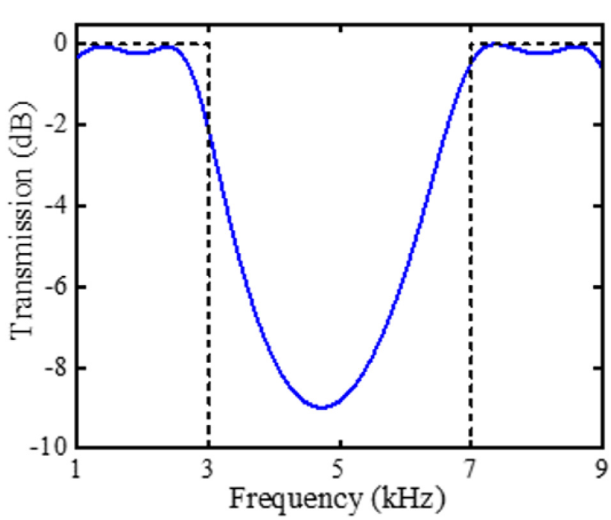

Fig. 10. Wave transmission from the continuous bandgap optimization of the active metabeam.

4. Conclusion

This study presents a physics-guided network based on machine learning (ML) algorithms for the efficient design of active metabeams. The physics-guided network is demonstrated to achieve user-defined dynamic wave functions and target the inverse design of non-periodic active metamaterials. The transfer matrix which relates the wave field and its derivative to govern the fundamental wave propagation in the metabeam will be embedded in the ML network to build up the complex mapping between the input and output wave responses. The ML-based neural network is proposed to learn the dynamic behavior of a class of metabeam units so that the prediction of the dynamic response for any unit in such class could be obtained without the need of time-consuming numerical simulation. The most remarkable characteristic of this approach lies in the ability to build predictive models of complex dynamical systems from the use of previously trained networks that capture the dynamics of the metabeam. In this approach, the NN replaces conventional numerical simulations to solve wave propagation problem in the metabeam. Once the NNs are concatenated by assembling these transfer matrices together to build the global transfer matrix, the transmission response of the whole system can be

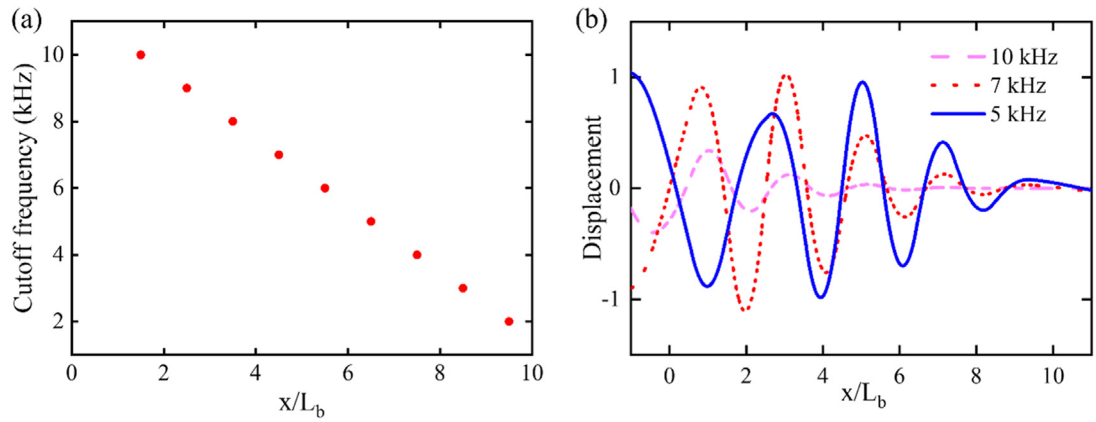

Fig. 11. (a) Target cutoff frequency of each unit cell along the metabeam. (b) The transverse displacement field along the metabeam at different frequencies.

obtained by following assigned input conditions and material and NC properties. During the inverse design stage, the NCs of each individual unit are treated as the design parameters to be solved by employing the surrogate optimization to minimize the difference between the responses estimated from the concatenated networks and the targeted wave responses. This approach is validated through a system consisting in a 1D active metabeam, and promising multifunctional wave control abilities are obtained to demonstrate the robustness of the proposed approach. The surrogate optimization based on ML networks can significantly speed up the inverse design while keeping the reconstructed transmission curve agree well with the target at the same time, which is ten time faster than the conventional optimization. The ML-guided surrogate optimization developed for inverse design of active metamaterials with a high dimension (2D or 3D) can find important applications in fast inverse design of various multi-functional metamaterials.

Declaration of competing interest

The authors declare that they have no known competing financial interests or personal relationships that could have appeared to influence the work reported in this paper.

Data availability

Data will be made available on request.

Acknowledgments

This work is supported by the Air Force Office of Scientific Research, USA under Grant No. AF9550-18-1-0342 and AF 9550-20-0279 with Program Manager Dr. Byung-Lip (Les) Lee and the Army Research Office, USA under Grant No. W911NF-18-1-0031 with Program Manager Dr. Daniel P Cole.

Appendix A. Assembly of global stiffness matrix

A stiffness matrix $\mathbf{D}(\omega, \lambda_N)$ of a unit with negative capacitance ratio λ_N relates the force vector $\mathbf{f}(\omega, \lambda_N) = [-M_L,\ -F_L,\ M_R,\ F_R]^T$ and displacement vector $\mathbf{u}(\omega, \lambda_N) = [w_L,\ \theta_L,\ w_R,\ \theta_R]^T$ as

$$\mathbf{f}(\omega, \lambda_N) = \mathbf{D}(\omega, \lambda_N)\mathbf{u}(\omega, \lambda_N) \tag{A.1}$$

and the stiffness matrix $\mathbf{D}(\omega, \lambda_N)$ can be obtained from the transfer matrix $\mathbf{Q}(\omega, \lambda_N)$ via:

$$\mathbf{D} = \begin{bmatrix} \mathbf{D}_{LL} & \mathbf{D}_{LR} \\ \mathbf{D}_{RL} & \mathbf{D}_{RR} \end{bmatrix} = \begin{bmatrix} \mathbf{Q}_{12}^{-1}\mathbf{Q}_{11} & -\mathbf{Q}_{12}^{-1} \\ \mathbf{Q}_{21} - \mathbf{Q}_{22}\mathbf{Q}_{12}^{-1}\mathbf{Q}_{11} & \mathbf{Q}_{22}\mathbf{Q}_{12}^{-1} \end{bmatrix} \tag{A.2}$$

with $\mathbf{Q}_{11}$, $\mathbf{Q}_{12}$, $\mathbf{Q}_{21}$ and $\mathbf{Q}_{22}$ being the submatrices of the transfer matrix $\mathbf{Q}$:

$$\mathbf{Q} = \begin{bmatrix} \mathbf{Q}_{11} & \mathbf{Q}_{12} \\ \mathbf{Q}_{21} & \mathbf{Q}_{22} \end{bmatrix} \tag{A.3}$$

As is shown in Fig. 1(a), PMLs have been added to the left end and right end of the beam system. The boundary conditions representing these PMLs can be expressed as :

$$\mathbf{f}_{GL} = \mathbf{D}_{GL}\mathbf{u}_{GL}$$
$$\mathbf{f}_{GR} = \mathbf{D}_{GR}\mathbf{u}_{GR}$$

with

$$\mathbf{D}_{GL} = -EI\kappa \begin{bmatrix} i\kappa & -1-i \\ (1-i)\kappa^2 & i\kappa \end{bmatrix}$$
$$\mathbf{D}_{GR} = -EI\kappa \begin{bmatrix} i\kappa & 1+i \\ -(1-i)\kappa^2 & i\kappa \end{bmatrix}$$

where $\kappa = \sqrt[4]{\rho S\omega^2/EI}$ is the wavenumber of the substrate beam at frequency ω, S is the area of its cross section, EI is its bending stiffness, the subscript GL or GR stands for the left or right end of the global system, respectively, and $\mathbf{f}_{GL} = [M_{GL},\ F_{GL}]^T$, $\mathbf{u}_{GL} = [w_{GL},\ \theta_{GL}]^T$, $\mathbf{f}_{GR} = [-M_{GL},\ -F_{GL}]^T$ and $\mathbf{u}_{GR} = [w_{GR},\ \theta_{GR}]^T$.

Then, by using the continuous boundary conditions at the interfaces in the system, we can assembly the stiffness relation together to get the global stiffness relation that relates the global nodal force $\mathbf{f}_G$ and global nodal displacement $\mathbf{u}_G$ as

$$\mathbf{f} = \mathbf{K}\mathbf{u} \tag{A.4}$$

with

$$\mathbf{f} = [\mathbf{f}_{GL} \quad \mathbf{0} \quad \mathbf{0} \quad \cdots \quad \mathbf{0}]^T$$
$$\mathbf{u} = [\mathbf{u}_{L1} \quad \mathbf{u}_{R1} \quad \mathbf{u}_{R2} \quad \cdots \quad \mathbf{u}_{RN}]^T$$

and the global stiffness matrix $\mathbf{K}$ as

$$\mathbf{K} = \begin{bmatrix} \mathbf{D}_{GL} + \mathbf{D}_{RR}^1 & \mathbf{D}_{LR}^1 & \mathbf{0} & \cdots & \mathbf{0} & \mathbf{0} \\ \mathbf{D}_{RL}^1 & \mathbf{D}_{RR}^1 + \mathbf{D}_{LL}^2 & \mathbf{D}_{LR}^2 & \ddots & \ddots & \mathbf{0} \\ \mathbf{0} & \mathbf{D}_{RL}^2 & \mathbf{D}_{RR}^2 + \mathbf{D}_{LL}^3 & \ddots & \ddots & \vdots \\ \vdots & \ddots & \ddots & \ddots & \ddots & \vdots \\ \mathbf{0} & \ddots & \ddots & \ddots & \mathbf{D}_{RR}^{N-1} + \mathbf{D}_{LL}^N & \mathbf{D}_{LR}^N \\ \mathbf{0} & \mathbf{0} & \mathbf{0} & \cdots & \mathbf{D}_{RL}^N & \mathbf{D}_{RR}^N + \mathbf{D}_{GR} \end{bmatrix} \tag{A.5}$$

Without loss of generality, we can assume that the system is excited by a point force f_E, then we can write $\mathbf{f}_{GL} = [0,\ f_E]^T$, then

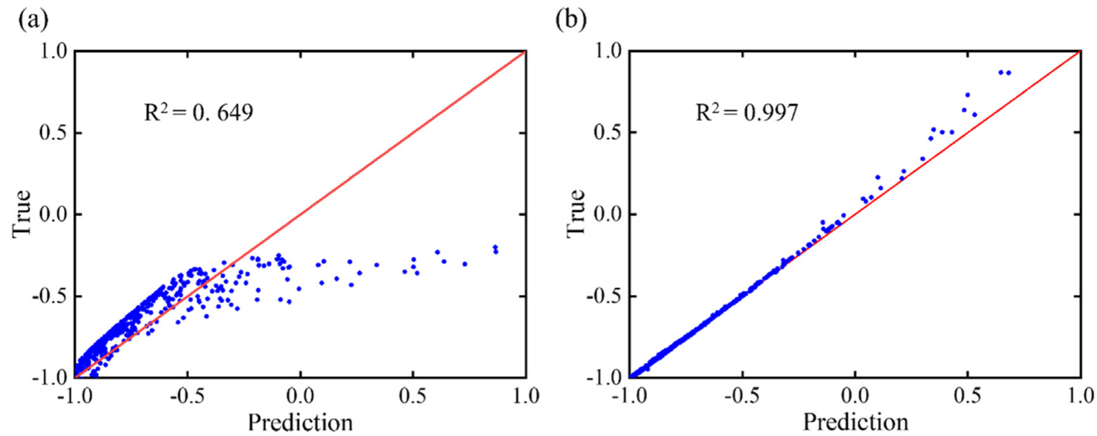

Fig. 12. The R^2 regression by using (a) linear regression and (b) ANN trained with Adam optimizer.

from the global stiffness relation Eq. (A.4), we can calculate the global nodal displacement, from which we can finally obtain the wave transmission and the mode shape of the system.

Appendix B. Comparison of prediction accuracy with standard methods

We compare current ML model with linear regression and ANN trained with Adam optimizer. The R^2 coefficients of lather two can be found in Fig. 12. As shown in figure, the linear regression model is unable to accurately predict the exact transfer matrix. Meanwhile, ANN with Adam optimizer can predict the matrix elements accurately as R^2 coefficient up to 0.997. However, this is not sufficient for predicting the transfer matrix since the error from the predicted matrix would quickly accumulate and amplify as we perform further calculations to predict resulting wave phenomena. For this reason, we choose to train ANN with Levenberg–Marquardt optimizer to minimize prediction error.

References

[1] X. Jiang, Y. Li, D. Ta, W. Wang, Ultrasonic sharp autofocusing with acoustic metasurface, Phys. Rev. B 102 (6) (2020) 064308.
[2] S. Zhang, C. Xia, N. Fang, Broadband acoustic cloak for ultrasound waves, Phys. Rev. Lett. 106 (2) (2011) 024301.
[3] D. Lu, Z. Liu, Hyperlenses and metalenses for far-field super-resolution imaging, Nature Commun. 3 (1) (2012) 1–9.
[4] J. Li, C.T. Chan, Double-negative acoustic metamaterial, Phys. Rev. E 70 (5) (2004) 055602.
[5] Y. Zhang, Z. Sha, G. Su, H. Zhou, P. Jiang, Y. Liu, B. Li, T. Wang, Ultra-compact metafence to block and channel mechanical waves, Extreme Mech. Lett. 52 (2022) 101659.
[6] Y. Chen, G. Hu, G. Huang, An adaptive metamaterial beam with hybrid shunting circuits for extremely broadband control of flexural waves, Smart Mater. Struct. 25 (10) (2016) 105036.
[7] A. Minovich, D.N. Neshev, D.A. Powell, I.V. Shadrivov, Y.S. Kivshar, Tunable fishnet metamaterials infiltrated by liquid crystals, Appl. Phys. Lett. 96 (19) (2010) 193103.
[8] D. Yang, L. Jin, R.V. Martinez, K. Bertoldi, G.M. Whitesides, Z. Suo, Phase-transforming and switchable metamaterials, Extreme Mech. Lett. 6 (2016) 1–9.
[9] A.M. Baz, An active acoustic metamaterial with tunable effective density, J. Vib. Acoust. 132 (4) (2010).
[10] X. Li, Y. Chen, X. Zhang, G. Huang, Shaping elastic wave mode conversion with a piezoelectric-based programmable meta-boundary, Extreme Mech. Lett. 39 (2020) 100837.
[11] Y. Chen, G. Huang, C. Sun, Band gap control in an active elastic metamaterial with negative capacitance piezoelectric shunting, J. Vib. Acoust. 136 (6) (2014).
[12] H. Zhang, J. Wen, Y. Xiao, G. Wang, X. Wen, Sound transmission loss of metamaterial thin plates with periodic subwavelength arrays of shunted piezoelectric patches, J. Sound Vib. 343 (2015) 104–120.
[13] J. Marconi, E. Riva, M. Di Ronco, G. Cazzulani, F. Braghin, M. Ruzzene, Experimental observation of nonreciprocal band gaps in a space-time-modulated beam using a shunted piezoelectric array, Phys. Rev. A 13 (3) (2020) 031001.
[14] R. Zhu, Y. Chen, M.V. Barnhart, G. Hu, C. Sun, G. Huang, Experimental study of an adaptive elastic metamaterial controlled by electric circuits, Appl. Phys. Lett. 108 (1) (2016) 011905.
[15] L. Airoldi, M. Ruzzene, Design of tunable acoustic metamaterials through periodic arrays of resonant shunted piezos, New J. Phys. 13 (11) (2011) 113010.
[16] W. Zhou, W. Chen, Z. Chen, C. Lim, et al., Actively controllable flexural wave band gaps in beam-type acoustic metamaterials with shunted piezoelectric patches, Eur. J. Mech. A Solids 77 (2019) 103807.
[17] C.J. Rupp, A. Evgrafov, K. Maute, M.L. Dunn, Design of phononic materials/structures for surface wave devices using topology optimization, Struct. Multidiscip. Optim. 34 (2) (2007) 111–121.
[18] Z. Du, H. Chen, G. Huang, Optimal quantum valley Hall insulators by rationally engineering Berry curvature and band structure, J. Mech. Phys. Solids 135 (2020) 103784.
[19] G.A. Gazonas, D.S. Weile, R. Wildman, A. Mohan, Genetic algorithm optimization of phononic bandgap structures, Int. J. Solids Struct. 43 (18–19) (2006) 5851–5866.
[20] O.R. Bilal, M.I. Hussein, Ultrawide phononic band gap for combined in-plane and out-of-plane waves, Phys. Rev. E 84 (6) (2011) 065701.
[21] S. Nanthakumar, X. Zhuang, H.S. Park, C. Nguyen, Y. Chen, T. Rabczuk, Inverse design of quantum spin Hall-based phononic topological insulators, J. Mech. Phys. Solids 125 (2019) 550–571.
[22] A. Bacigalupo, G. Gnecco, M. Lepidi, L. Gambarotta, Machine-learning techniques for the optimal design of acoustic metamaterials, J. Optim. Theory Appl. 187 (3) (2020) 630–653.
[23] X. Li, S. Ning, Z. Liu, Z. Yan, C. Luo, Z. Zhuang, Designing phononic crystal with anticipated band gap through a deep learning based data-driven method, Comput. Methods Appl. Mech. Engrg. 361 (2020) 112737.
[24] W. Ma, F. Cheng, Y. Xu, Q. Wen, Y. Liu, Probabilistic representation and inverse design of metamaterials based on a deep generative model with semi-supervised learning strategy, Adv. Mater. 31 (35) (2019) 1901111.
[25] Y. Chen, X. Li, C. Scheibner, V. Vitelli, G. Huang, Realization of active metamaterials with odd micropolar elasticity, Nature Commun. 12 (1) (2021) 1–12.
[26] Y. Jin, L. He, Z. Wen, B. Mortazavi, H. Guo, D. Torrent, B. Djafari-Rouhani, T. Rabczuk, X. Zhuang, Y. Li, Intelligent on-demand design of phononic metamaterials, Nanophotonics (2022).
[27] R.-T. Wu, T.-W. Liu, M.R. Jahanshahi, F. Semperlotti, Design of one-dimensional acoustic metamaterials using machine learning and cell concatenation, Struct. Multidiscip. Optim. 63 (5) (2021) 2399–2423.
[28] L. Wu, L. Liu, Y. Wang, Z. Zhai, H. Zhuang, D. Krishnaraju, Q. Wang, H. Jiang, A machine learning-based method to design modular metamaterials, Extreme Mech. Lett. 36 (2020) 100657.
[29] J. Zhang, Y. Li, T. Zhao, Q. Zhang, L. Zuo, K. Zhang, Machine-learning based design of digital materials for elastic wave control, Extreme Mech. Lett. 48 (2021) 101372.
[30] Y. LeCun, Y. Bengio, G. Hinton, Deep learning, Nature 521 (7553) (2015) 436–444.
[31] E. Samaniego, C. Anitescu, S. Goswami, V.M. Nguyen-Thanh, H. Guo, K. Hamdia, X. Zhuang, T. Rabczuk, An energy approach to the solution of partial differential equations in computational mechanics via machine learning: Concepts, implementation and applications, Comput. Methods Appl. Mech. Engrg. 362 (2020) 112790.

[32] C. Anitescu, E. Atroshchenko, N. Alajlan, T. Rabczuk, Artificial neural network methods for the solution of second order boundary value problems, Comput. Mater. Contin. 59 (1) (2019) 345–359.
[33] Y. Chen, R. Zhu, M.V. Barnhart, G. Huang, Enhanced flexural wave sensing by adaptive gradient-index metamaterials, Sci. Rep. 6 (1) (2016) 1–11.
[34] N.W. Hagood, A. Von Flotow, Damping of structural vibrations with piezoelectric materials and passive electrical networks, J. Sound Vib. 146 (2) (1991) 243–268.
[35] J.a.F. Henriques, S. Ehrhardt, S. Albanie, A. Vedaldi, Small steps and giant leaps: Minimal newton solvers for deep learning, in: Proceedings of the IEEE/CVF International Conference on Computer Vision, 2019, pp. 4763–4772.
[36] Y. Jin, Y. Pennec, B. Djafari-Rouhani, Acoustic analogue of electromagnetically induced transparency and Autler–Townes splitting in pillared metasurfaces, J. Phys. D: Appl. Phys. 51 (49) (2018) 494004.
[37] A. Korovin, Y. Pennec, B. Djafari-Rouhani, Strong coupling of phononic cavity modes in one-dimensional corrugated nanobeam structures, Phys. Rev. B 96 (18) (2017) 184302.
[38] J.M. Kweun, H.J. Lee, J.H. Oh, H.M. Seung, Y.Y. Kim, Transmodal Fabry-Pérot resonance: theory and realization with elastic metamaterials, Phys. Rev. Lett. 118 (20) (2017) 205901.
[39] J. Zhu, Y. Chen, X. Zhu, F.J. Garcia-Vidal, X. Yin, W. Zhang, X. Zhang, Acoustic rainbow trapping, Sci. Rep. 3 (1) (2013) 1–6.
[40] C. Zhou, B. Yuan, Y. Cheng, X. Liu, Precise rainbow trapping for low-frequency acoustic waves with micro mie resonance-based structures, Appl. Phys. Lett. 108 (6) (2016) 063501.
[41] J. Xu, S. Xiao, P. He, Y. Wang, Y. Shen, L. Hong, Y. Luo, B. He, Realization of broadband truly rainbow trapping in gradient-index metamaterials, Opt. Express 30 (3) (2022) 3941–3953.